Quantitative Elucidation of Catalytic Reaction of Truncated Aldehyde Dehydrogenase Based on Linear Free Energy Relationship

Konatsu Ichikawa, Taiki Adachi*, Yuki Kitazumi, Osamu Shirai, and Keisei Sowa*

Division of Applied Life Sciences, Graduate School of Agriculture, Kyoto University, Sakyo, Kyoto 606-8502, Japan

KEYWORDS: Bioelectrocatalysis, Direct electron transfer, Aldehyde dehydrogenase, Kinetic analysis, Linear free energy relationship

ABSTRACT: Some oxidoreductases can communicate directly and electrically with electrodes; this process is called direct electron transfer (DET)-type bioelectrocatalysis. Understanding its detailed mechanisms is essential for developing and improving DET-based bioelectrochemical devices. In this study, we investigated the pH dependence of kinetic and thermodynamic characteristics of a variant of an aldehyde dehydrogenase (ALDH) without the cytochrome *c* subunit (ΔC_ALDH) and compared it with that of a wild-type recombinant ALDH (rALDH). Owing to the pronounced DET activity of ΔC_ALDH at multi-walled carbon nanotubes, the voltammograms were analyzed to obtain the enzymatic parameters. The potential difference between the electrode-active site of the enzyme and electron donor ($E^{\circ\prime}_{\mathrm{E}} - E^{\circ\prime}_{\mathrm{D}}$) and the limiting catalytic current density (j_{cat}) exhibited an ideal linear free energy relationship (LFER), suggesting that the catalytic reaction of ΔC_ALDH was controlled by the thermodynamic driving force without any specific interactions. We also measured the ferricyanide reductase activity in solution (k_{sol}) to investigate the effect of electron acceptors (electrode and ferricyanide) on the enzymatic properties. The k_{sol} of ΔC_ALDH has a pH dependence similar to that of j_{cat}; therefore, the experimental data were kinetically analyzed based on the LFER by considering the potential difference between the electron acceptor and electrode-active site of the enzyme ($E^{\circ\prime}_{\mathrm{A}} - E^{\circ\prime}_{\mathrm{E}}$). By integrating the analytical results obtained from the DET-type acetaldehyde oxidation using an electrode and ferricyanide reduction in solution, the catalytic constant for the DET-type bioelectrocatalysis (k_{DET}) and the surface concentration of the effective enzyme immobilized on the electrode ($\Gamma_{\mathrm{E,eff}}$) of ΔC_ALDH were calculated to be 5000 ± 2000 s^{-1} and 13 ± 7 pmol cm^{-2}, respectively. This study achieved a detailed evaluation of the multi-step catalytic reactions of redox enzymes and can help elucidate the reaction mechanisms of DET-type bioelectrocatalysis.

1. INTRODUCTION

In vivo, oxidoreductases are essential catalysts for biological electron transfer (ET) reactions such as respiration, photosynthesis, and fermentation. These enzymatic reactions can be artificially coupled with electrode reactions, which is a process known as bioelectrocatalysis, and are classified into two types: mediated ET (MET) and direct ET (DET) reactions.[1–8] Oxidoreductases can communicate directly with electrodes in DET-type reactions, while artificial electron mediators are additionally required for MET-type reactions.[9–14] Owing to advantages such as energy efficiency, biocompatibility, and design flexibility, the mediator-less DET-type reactions are expected to be applied to bioelectrochemical devices such as biosensors,[15–27] biofuel cells,[27–34] and bioreactors.[35–37]

To achieve more efficient DET-type reactions, their mechanisms have been studied from the perspective of structural biology, bioelectrochemistry, and computational science.[11,33,38–42] In particular, various types of enzymatic information can be obtained by kinetically analyzing the DET-type voltammograms. According to the simplest model for a DET-type reaction,[43] the steady-state catalytic current density in oxidation (j) is given by Equation (1).

$$j = \frac{j_{\mathrm{cat}}}{1 + \eta^{-(1-\alpha)}\left(\frac{k^{\circ}}{k_{\mathrm{DET}}}\right)^{-1} + \eta^{-1}} \quad (1)$$

where j_{cat} is the limiting catalytic current density; k_{DET} is the catalytic constant in the DET-type reaction (note that k_{DET} is not equal to the catalytic constant in solution); k° is the standard rate constant of the heterogeneous ET reaction; and α is the transfer coefficient (typically 0.5). k° depends exponentially on the distance between the electrode and electrode-active site of the enzyme (d), and is expressed using Equation (2).[44]

$$k^{\circ} = k^{\circ}{}_{\max} \exp\{-\beta(d - d_{\min})\} \quad (2)$$

j_{cat} and η are defined as shown in Equations (3) and (4), respectively.

$$j_{\mathrm{cat}} = n_{\mathrm{S}} F k_{\mathrm{DET}} \Gamma_{\mathrm{E,eff}} \quad (3)$$

$$\eta = \exp\left\{\frac{n'_{\mathrm{E}} F}{RT}(E - E^{\circ\prime}_{\mathrm{E}})\right\} \quad (4)$$

where $k^{\circ}{}_{\max}$ is the maximum k° at the closest approach ($d = d_{\min}$); β is the decay coefficient of the long-range ET (assumed to be 1.4 $Å^{-1}$ for proteins[45]); $\Gamma_{\mathrm{E,eff}}$ is the surface concentration of the effective enzyme on the electrode; n_{S} is the number of electrons involved in substrate oxidation; n'_{E} is

the number of electrons in the rate-determining step (RDS) of the heterogeneous ET (typically 1); E is the electrode potential; $E^{\circ\prime}_{E}$ is the formal potential of the electrode-active site of the enzyme; F is the Faraday constant; R is the gas constant; and T is the absolute temperature. In Equation (3), both k_{DET} and $\Gamma_{E,eff}$ are critical parameters for improving $j_{cat.}$ However, it is difficult to evaluate these factors separately. They can be estimated from the non-catalytic signals of the enzyme; that is, the amount of charge derived from the enzyme accessible to the electrode is converted into $\Gamma_{E,eff}$.[9] This method is applicable only under the conditions that $\Gamma_{E,eff}$ is large enough and that the orientation of the enzyme is suitable for DET.[9,46–48] Although porous electrode materials are somewhat effective in realizing such conditions,[46,49] distinguishing significant non-catalytic signals from background currents accurately is often difficult. Thus, a new analytical model is required to evaluate k_{DET} and $\Gamma_{E,eff}$ separately to further understand DET-type reactions.

We focused on aldehyde dehydrogenase (ALDH) from *Gluconobacter oxydans*, which is a membrane-bound protein that catalyzes DET-type acetaldehyde oxidation.[50–52] Its three-dimensional structure has been elucidated using cryo-electron microscopy analysis (PDB: 8GY3).[53] ALDH comprises a large catalytic subunit (L subunit; AldH), a small subunit (S subunit; AldG), and a membrane-bound cytochrome *c* subunit (C subunit; AldF) (Figure 1A). In vivo, electrons extracted from acetaldehyde are transferred to ubiquinone via the catalytic center (molybdenum cofactor, Moco) in the L subunit, two iron-sulfur clusters (FeSs) in the S subunit, and three heme *c* moieties in the C subunit, in this order. The ET associated with substrate oxidation via the C subunit is conserved in membrane-bound hemoproteins such as alcohol dehydrogenase (ADH),[51,52,54,55] glucose dehydrogenase (GDH),[56–60] and fructose dehydrogenase (FDH).[40,61–64] Research on ALDH contributes to a comprehensive understanding of the DET-type reactions catalyzed by these membrane-bound hemoproteins, because these enzymes have similarities in their high DET activities.

In previous studies, variants truncating the C subunit of ADH, FDH, and GDH, which are termed ΔC_ADH,[65] ΔC_FDH,[66–68] and ΔC_GDH,[69–72] respectively, have been investigated to clarify the functions of the C subunit. The soluble ΔC variants are advantageous in shortening purification processes and preventing the interference of detergents with their catalytic reactions. The ΔC variants showed lesser catalytic activities than their wild-type heterotrimers,

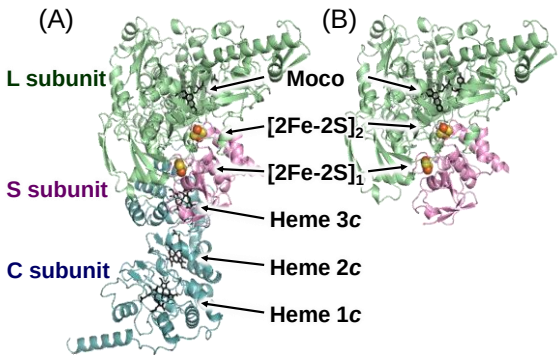

Figure 1. (A) 3D structure of rALDH (PDB: 8GY3) and (B) the putative structure of ΔC_ALDH; [green: L, magenta: S, and cyan: C subunits].

indicating the importance of the C subunits. These results suggest that the high catalytic activity can be attributed to the multi-step intramolecular ET via the heme *c* moieties. The structural characteristics of the ΔC variant of ALDH (ΔC_ALDH) are different from those of ΔC_ADH, ΔC_FDH, and ΔC_GDH; while ΔC_ALDH has three cofactors and two of these are present in the S subunit, the others have two cofactors only in the L subunit (Figure 1B). Thus, research on ΔC_ALDH is advantageous with respect to the multi-step intramolecular ET in the S subunit for elucidating the DET-type reaction mechanism of ALDH.

In this study, we constructed ΔC_ALDH, attempted to characterize its bioelectrochemical properties, and compared them with those of the wild-type recombinant ALDH (rALDH). Both enzymes were quantitatively investigated using bioelectrochemistry, with the primary focus on the pH dependence of their kinetic and thermodynamic parameters. In addition, their DET-type activities were compared with the activities of ferricyanide reduction in solution. By kinetically analyzing the two reactions with different electron acceptors (an electrode and ferricyanide), we propose a novel method for separately estimating k_{DET} and $\Gamma_{E,eff}$ without non-catalytic signals.

2. EXPERIMENTAL

2.1. Materials and chemicals. Multi-walled carbon nanotubes (MWCNTs, O.D.: 10 ± 1 nm, I.D.: 4.5 ± 0.5 nm, length: 3~6 μm) were purchased from Sigma-Aldrich Co. (USA). Protein markers and 12.5% acrylamide gels for sodium dodecyl sulfate polyacrylamide gel electrophoresis (SDS-PAGE) were obtained from Nacalai Tesque Inc. (Japan) and Atto Co. (Japan), respectively. A P′ medium was prepared with 1% yeast extract (Oriental Yeast Co., Ltd., Japan), 1% hipolypeptone (Shiotani M.S. Co., Ltd., Japan), 0.5% glucose, and 2% glycerol. All other chemicals were obtained from Wako Pure Chemical Industries Ltd. (Japan), unless otherwise stated. All aqueous solutions were prepared using ultrapure water.

2.2. Construction of plasmids and strains. The bacterial strains and plasmids used in this study are listed in Table S1. A knockout *G. oxydans* strain lacking ADH and ALDH genes (*adhAB* and *aldFGH*, respectively) was constructed by homologous recombination using pK18mobsacB-based suicide plasmids.[73] The homologous deoxyribonucleic acid (DNA) fragments located the upstream and downstream regions of the target genes (approximately 1 kbp each) were amplified by polymerase chain reaction (PCR) from the genomic DNA of a wild-type *G. oxydans* strain using a thermal cycler (T100, Bio-Rad, USA), DNA polymerase (KOD One® PCR Master Mix, Toyobo, Japan), and primer pairs (*adhAB*_up_f/*adhAB*_up_r, *adhAB*_down_f/*adhAB*_down_r, *aldFGH*_up_f/*aldFGH*_up_r, and *aldFGH*_down_f/*aldFGH*_down_r). The plasmid backbone was amplified by inverse PCR from pK18mobsacB using the primer pair (pK18mobsacB_inv_f/pK18mobsacB_inv_r). The primer sequences used in this study are listed in Table S2. To yield pK18mobsacB_Δ*adhAB* and pK18mobsacB_Δ*aldFGH*, the PCR products were assembled by in-fusion cloning using an NEBuilder® HiFi DNA Assembly Master Mix (New England BioLabs, USA). DH5α cells of *Escherichia coli* were used for plasmid construction. pK18mobsacB_Δ*adhAB* was first introduced into the wild-type *G. oxydans* strain by triparental

mating with the *E. coli* HB101 strain, which includes the pRK2013 plasmid.[74] A kanamycin-resistant transformant, obtained by first homologous recombination, was then cultivated on an agarose plate with a P′ medium containing 10% sucrose. A Δ*adhAB* variant was selected from sucrose-resistant transformants obtained by second homologous recombination. Deletion of the *adhAB* genes was confirmed by colony PCR analysis and gel electrophoresis. pK18mobsacB_Δ*aldFGH* was then introduced into the Δ*adhAB* strain to obtain a Δ*adhAB*Δ*aldFGH* variant by repeating the above-mentioned steps. The plasmids for overexpression of rALDH and ΔC_ALDH (pBBR1MCS-4-Padh-*aldFGH* and pBBR1MCS-4-Padh-*aldGH*, respectively) were finally introduced into the *G. oxydans* Δ*adhAB*Δ*aldFGH* strain by triparental mating. Preparation and confirmation of pBBR1MCS-4-Padh-*aldGH* were outsourced to Vector-Builder Japan Inc., Japan.

2.3. Expression and purification of rALDH and ΔC_ALDH. rALDH was purified using an improved protocol based on previous reports.[53,75] The pBBR1MCS-4-Padh-*aldFGH* strain was cultivated in a P′ medium with 100 μM Na_2MoO_4 to overexpress rALDH. The cells were collected by centrifugation at 10,000 × *g* for 5 min at 4 °C, resuspended in 20 mM acetate buffer (pH 5.5), and disrupted twice using a French Press cell disruptor (FA-080R, Thermo Fisher Scientific, USA) at 100 MPa. The suspension was centrifuged at 12,000 × *g* for 5 min at 4 °C to remove cell debris, the supernatant was centrifuged at 100,000 × *g* for 1 h at 4 °C, and the precipitate was collected as a membrane fraction. The precipitate was resuspended in 20 mM acetate buffer (pH 5.5) containing 50 mM benzaldehyde, 2% Triton® X-100, and 10% sucrose, using a glass homogenizer. The suspension was stirred for 10 h at 4 °C to solubilize rALDH, and subsequently centrifuged at 100,000 × *g* for 1 h at 4 °C. The supernatant was collected as a crude enzyme solution and loaded onto a TOYOPEARL® DEAE-650M column (approximately 20 mL, Tosoh Bioscience, Japan) equilibrated using a 20 mM acetate buffer (pH 5.5) containing 5 mM benzaldehyde, 0.1% Triton® X-100, and 10% sucrose. The column was washed with a 2.5-bed volume of the same buffer. The collected DEAE-passing fraction was loaded onto a TOYOPEARL® CM-650M column (approximately 20 mL, Tosoh Bioscience, Japan) equilibrated using the same buffer. The column was washed with a 5-bed volume of 20 mM acetate buffer (pH 5.5) containing 0.1% Triton® X-100 and 10% sucrose. A linear gradient elution with acetate buffer (pH 5.5) from 20 to 500 mM containing 0.1% Triton® X-100 and 10% sucrose was conducted, and fractions with acetaldehyde oxidation activity were collected as a purified enzyme solution, which was finally concentrated using 100 kDa ultrafiltration membranes and frozen in liquid nitrogen.

ΔC_ALDH was purified as follows: The pBBR1MCS-4-Padh-*aldGH* strain was cultivated in a P′ medium with 100 μM Na_2MoO_4 to overexpress ΔC_ALDH. The cells were collected by centrifugation at 10,000 × *g* for 5 min at 4 °C, resuspended in 20 mM acetate buffer (pH 5.0) containing 50 mM benzaldehyde and 10% sucrose, and disrupted twice using the French Press cell disruptor at 100 MPa. The suspension was centrifuged at 12,000 × *g* for 5 min at 4 °C to remove cell debris, while the supernatant was centrifuged at 100,000 × *g* for 1 h at 4 °C and collected as a crude enzyme solution. It was then loaded onto another TOYOPEARL® DEAE-650M column (approximately 20 mL) equilibrated using a 20 mM acetate buffer (pH 5.0) containing 5 mM benzaldehyde and 10% sucrose. The column was washed with a 2.5-bed volume of the same buffer. The collected DEAE-passing fraction was loaded onto a TOYOPEARL® CM-650M column (approximately 20 mL) equilibrated using the same buffer. The column was then washed with a 5-bed volume of the same buffer. A linear gradient elution with acetate buffer (pH 5.0) from 20 to 500 mM containing 5 mM benzaldehyde and 10% sucrose was conducted, and fractions with acetaldehyde oxidation activity were collected. Ammonium sulfate was added to the collected fraction at a final concentration of 20% and gently stirred. The solution was loaded onto a TOYOPEARL® Butyl-650M column (approximately 20 mL) equilibrated using a 20 mM acetate buffer (pH 5.0) containing 5 mM benzaldehyde, 10% sucrose, and 20% ammonium sulfate. The column was then washed with a 5-bed volume of 20 mM acetate buffer (pH 5.0) containing 10% sucrose and 20% ammonium sulfate. A linear gradient elution with ammonium sulfate from 20 to 0% in 20 mM acetate buffer (pH 5.0) containing 10% sucrose was conducted, and fractions with acetaldehyde oxidation activity were collected as a purified enzyme solution, which was finally concentrated using 10 kDa ultrafiltration membranes and frozen in liquid nitrogen.

The concentrations of purified enzymes were estimated using a Pierce™ bicinchoninic acid (BCA) protein assay kit (Thermo Fisher Scientific Inc., USA), using bovine serum albumin as the standard sample. SDS-PAGE analysis was conducted to check the purity of the enzyme solutions (Figure S1). The band at 51 kDa corresponding to the C subunit was deficient in the lane of ΔC_ALDH, as expected.

2.4. Electrode preparation. Glassy carbon electrodes (GCEs, 3 mm in diameter, BAS Inc., Japan) were polished successively with a 1.0- and 0.05-μm alumina slurry, and first sonicated in and subsequently washed with distilled water. A 0.1-wt% MWCNT dispersion was prepared using *N*-methyl-2-pyrrolidone (NMP) by sonication for 2 h. A 10-μL aliquot of the MWCNT dispersion was applied onto the GCEs and dried at 70 °C. These electrodes were referred to as CNT/GCEs. NMP (2 μL) was dropped onto the electrodes to decrease the hydrophobicity of the electrode surface. After excess NMP was removed, a 20-μL aliquot of the enzyme solution (1 mg mL^{-1}) dissolved in 100 mM acetate buffer (pH 5.5 for rALDH and pH 5.0 for ΔC_ALDH) was applied onto the surface of the electrodes. The electrodes were placed in a water-saturated atmosphere for 2 h at 4 °C. These working electrodes were referred to as rALDH/CNT/GCE and ΔC_ALDH/CNT/GCE.

2.5. Electrochemical measurements. Electrochemical measurements were conducted using an electrochemical analyzer (ALS650E, BAS Inc., Japan) and a rotating disk electrode instrument (RRDE-3A, BAS Inc., Japan). A platinum wire and homemade Ag|AgCl|sat. KCl electrodes were used as the counter and reference electrodes, respectively. All the potentials in this study were recorded against the reference electrodes. All electrochemical measurements were performed in McIlvaine buffer under Ar-saturated conditions at 25 °C, scan rate (v) of 10 mV s^{-1}, and rotation speed (ω) of 4,000 rpm.

2.6. Enzyme assay. The activities of rALDH and ΔC_ALDH in solution were investigated spectrophotometrically using ferricyanide as an electron acceptor, according to a

previously reported procedure[50] with minor modifications. The enzyme assay was conducted using 800 µL of McIlvaine buffer containing 100 mM acetaldehyde and 50 mM potassium ferricyanide for 5 min at 25 °C. Subsequently, 400 µL of ferric sulfate-dupanol reagent,[50] which forms Prussian-blue with ferrocyanide, was added to stop the enzymatic reaction. After overnight incubation in the dark at 30 °C, the absorbance of the resulting Prussian-blue color was measured at 660 nm (A_{660}) using a cell with a 1-cm optical path length. Based on the linear relationship between the concentration of ferrocyanide and A_{660} of Prussian-blue, the slope of the calibration curve was calculated to be 5.04 ± 0.02 mM^{-1} in the concentration range below 10 mM ferrocyanide (Figure S2). One unit is defined as the amount of the enzyme that reacts with 1 µmol of acetaldehyde (or 2 µmol ferricyanide) per minute.

3. RESULTS AND DISCUSSIONS

3.1. Bioelectrochemical characterization of rALDH and ΔC_ALDH. Figure 2 shows the cyclic voltammograms (CVs) recorded at the rALDH/CNT/GCE and ΔC_ALDH/CNT/GCE. Both electrodes showed clear catalytic signals for the DET-type acetaldehyde oxidation, whereas non-catalytic signals derived from the adsorbed enzymes were not clearly observed. Based on the structural information, the electrode-active site of ΔC_ALDH is possibly estimated as $[2Fe\text{-}2S]_1$, because it is located closest to the surface of the enzyme among its cofactors (Figure 1B). Figure 3 shows the pH dependence of the DET activities of rALDH and ΔC_ALDH. The voltammograms were kinetically analyzed to determine the enzymatic properties. In this case, n_S in Equation (3) is defined as 2. Considering the distribution of the enzyme orientation on the electrode, we assumed three k° values (k°_1, k°_2, and k°_3),[76,77] and the proportion of enzymes with these k° values was set to p_1, p_2, and p_3 (= 1 – p_1 – p_2), respectively. Therefore, Equation (1) can be rewritten as shown in Equation (5).

$$j = j_{\mathrm{cat}} \sum_{n=1}^{3} p_n \left\{ 1 + \eta^{-(1-\alpha)} \left(\frac{k^\circ_n}{k_{\mathrm{DET}}} \right)^{-1} + \eta^{-1} \right\}^{-1} \qquad (5)$$

Considering that the long-range ET primarily occurs within 14 Å,[78] and that $[2Fe\text{-}2S]_1$ is approximately 9 Å farther from the surface of the enzyme (Figure S3), the distribution of the orientation of the enzyme involved in DET appears to be limited within approximately 5 Å. Based on Equation (2), d_{min}, d_{min} + 2.5 Å, and d_{min} + 5 Å correspond to k°_{max}, $k^\circ_{\mathrm{max}}/10^{1.5}$, and $k^\circ_{\mathrm{max}}/10^3$, respectively. Thus, we defined k°_1, k°_2, and k°_3 as k°_{max}, $k^\circ_{\mathrm{max}}/10^{1.5}$, and $k^\circ_{\mathrm{max}}/10^3$, respectively. Although the electrode-active site of rALDH has not yet been identified, we applied the same assumption to rALDH for comparing the two enzymes.

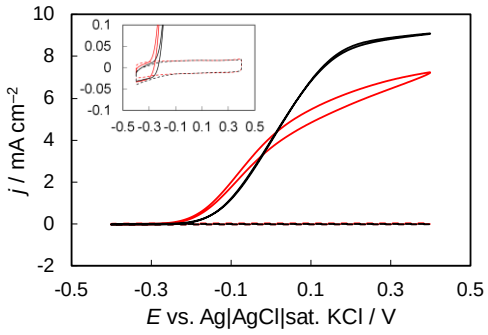

Figure 2. CVs for acetaldehyde oxidation at the rALDH/CNT/GCE (black) and ΔC_ALDH/CNT/GCE (red) in McIlvaine buffer (pH 5.0) in the presence of 100 mM acetaldehyde (solid lines). The broken lines represent the CVs at the rALDH/CNT/GCE and ΔC_ALDH/CNT/GCE without 100 mM acetaldehyde. The inset shows the enlarged CVs.

Using $E^{\circ\prime}_{\mathrm{E}}$, j_{cat}, $k^\circ_{\mathrm{max}}/k_{\mathrm{DET}}$, p_1, and p_2 as adjustable parameters, Equation (5) was fitted to the background-subtracted voltammograms by non-linear least-squares analysis in Gnuplot®. The refined parameters of rALDH and ΔC_ALDH are graphically summarized in Figures 4 and 5, respectively. The fitting results are shown in Figure S4. As the condition got basic, the $E^{\circ\prime}_{\mathrm{E}}$ values of both enzymes linearly decreased and reached a plateau. The j_{cat} values also showed similar but slightly different pH dependence for both enzymes; the j_{cat} values of rALDH increased as the pH conditions changed from acidic to neutral and reached a maximum at pH 7.5, while those of ΔC_ALDH exponentially increased with increasing pH from 2.5 to 5.5 and reached a plateau between pH 6.0 and 8.0. In the case of rALDH, no significant changes were observed in the $k^\circ_{\mathrm{max}}/k_{\mathrm{DET}}$ values, and the proportion of p_2 was the largest at all pH values investigated. In contrast, $k^\circ_{\mathrm{max}}/k_{\mathrm{DET}}$ decreased in the case of ΔC_ALDH, as the conditions changed to basic, and the proportion of p_1 was the largest. These results suggest that the distribution of the enzyme orientation is different in the cases of rALDH and ΔC_ALDH, possibly because of a difference in the sizes and shapes of the enzymes and interactions with the electrode. In addition, the rALDH enzyme solution contained Triton® X-100 as the solubilizer. A previous research reported that

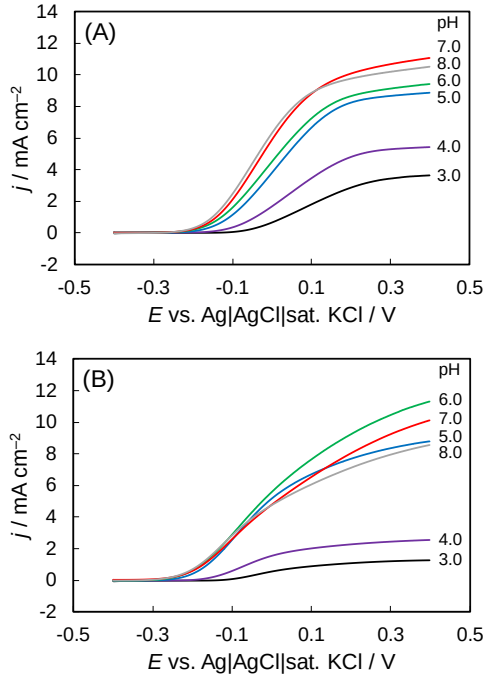

Figure 3. Background-subtracted linear sweep voltammograms for acetaldehyde oxidation at the (A) rALDH/CNT/GCE and (B) ΔC_ALDH/CNT/GCE at pH = 3.0 (black), 4.0 (purple), 5.0 (blue), 6.0 (green), 7.0 (red), and 8.0 (grey).

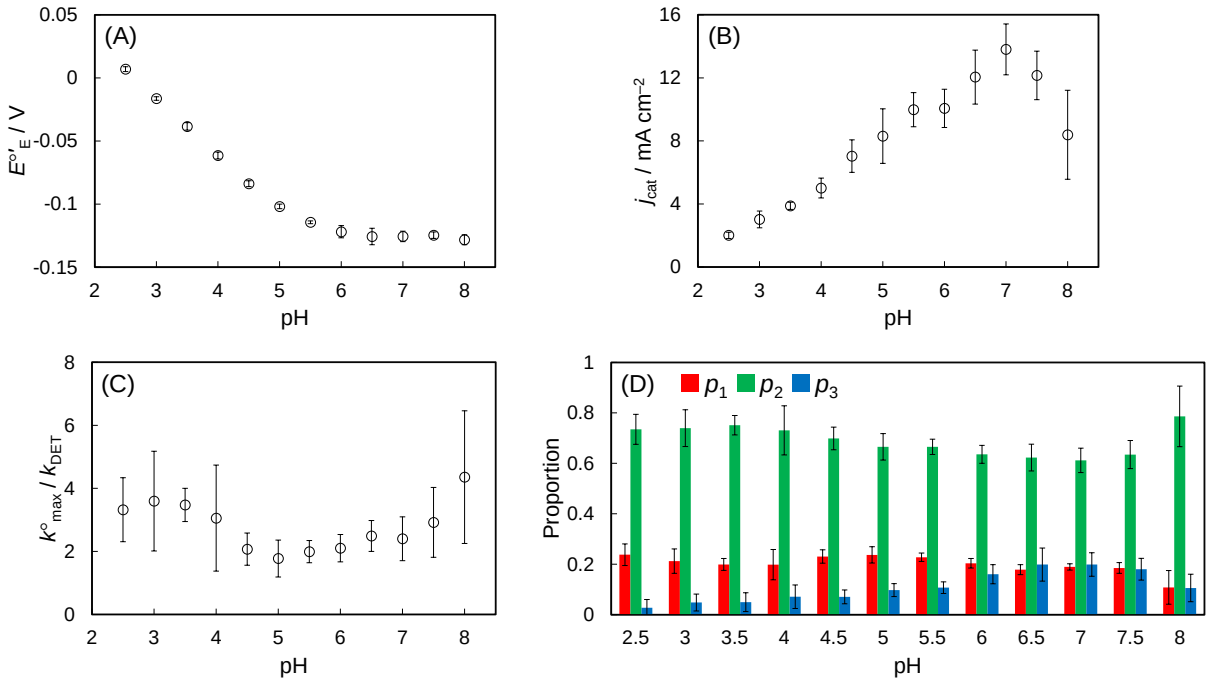

Figure 4. Graphical comparison of the refined parameters of rALDH. (A) $E^{\circ\prime}_E$, (B) j_{cat}, (C) k°_{max}/k_{DET}, and (D) p_1, p_2, and p_3. Errors were determined using the Student's t distribution at 90% confidence level (n = 6).

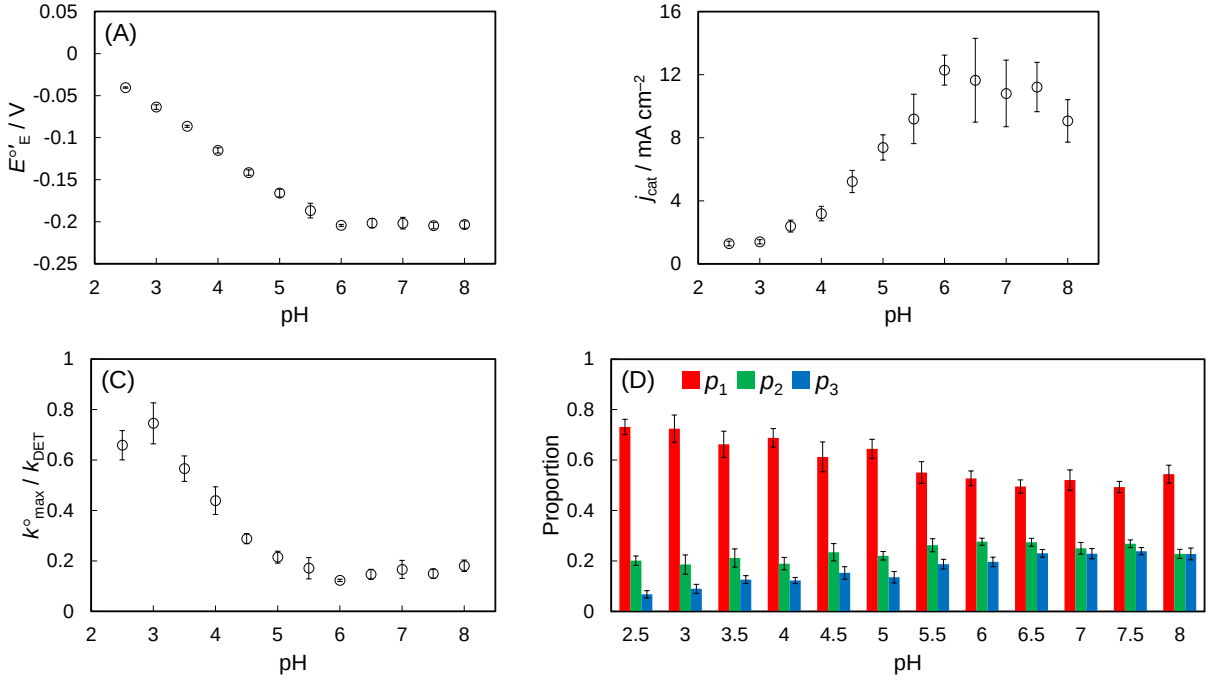

Figure 5. Graphical comparison of the refined parameters of ΔC_ALDH. (A) $E^{\circ\prime}_E$, (B) j_{cat}, (C) k°_{max}/k_{DET}, and (D) p_1, p_2, and p_3. Errors were determined using the Student's t distribution at 90% confidence level (n = 6).

considering the detergent interference in the DET-type reaction,[79] Triton® X-100 might affect the adsorption and distribution of rALDH.

3.2. Discussion on intramolecular ET based on linear free energy relationship (LFER). In this section, we have discussed the enzymatic properties (j_{cat} and $E^{\circ\prime}_E$) in greater detail. The redox reaction of acetate/acetaldehyde can be expressed using Equation (6).[50]

$$CH_3CHO + H_2O \rightleftarrows CH_3COO^- + 3H^+ + 2e^- \quad (6)$$

Figure 6 shows a comparison of the $E^{\circ\prime}_E$ values of rALDH and ΔC_ALDH and the formal potentials of the electron donor (acetate/acetaldehyde; $E^{\circ\prime}_D$: –0.778 V at pH 7.0[80]) and an artificial electron acceptor in solution (ferricyanide/ferrocyanide; $E^{\circ\prime}_A$: 0.171 V (independent of pH) [81]). In the plateaued region at neutral pH, the $E^{\circ\prime}_E$ values of ΔC_ALDH and rALDH were –0.204 ± 0.001 and –0.125 ± 0.001 V,

respectively, which indicated that ΔC_ALDH reduced the overpotential for acetaldehyde oxidation by approximately 80 mV. In addition, Equation (6) suggests that the pH dependence of $E^{\circ\prime}_D$ is –89 mV pH^{-1}, while the slopes of $E^{\circ\prime}_E$ of rALDH and ΔC_ALDH are approximately –50 mV pH^{-1}. Thus, $E^{\circ\prime}_E - E^{\circ\prime}_D$ increases as the conditions become more basic. Based on LFER theory, we focused on the relationship between $E^{\circ\prime}_E - E^{\circ\prime}_D$ and j_{cat}. Using the empirical formula for the LFER, the relationship between $E^{\circ\prime}_E - E^{\circ\prime}_D$ and k_{DET} can be expressed using Equation (7).[82,83]

$$\log\left(\frac{k_{\mathrm{DET},j}}{k_{\mathrm{DET},i}}\right) = \frac{\gamma n_{\mathrm{RDS}} F}{2.303RT}\Delta(E^{\circ\prime}_E - E^{\circ\prime}_D)_{j/i} \qquad (7)$$

where γ is the proportional constant in the LFER (ideally 0.5); n_{RDS} is the number of electrons in the RDS (assumed to be 1); and $\Delta(E^{\circ\prime}_E - E^{\circ\prime}_D)_{j/i}$ is the difference between the $E^{\circ\prime}_E - E^{\circ\prime}_D$ values of states i and j. Assuming that $E^{\circ\prime}_E = E^{\circ\prime}_D$ and $k_{DET,i} = k_{DET,0}$ at the state i, Equation (7) can be rewritten to obtain Equation (8).

$$\log\left(\frac{k_{\mathrm{DET}}}{k_{\mathrm{DET},0}}\right) = \frac{\gamma n_{\mathrm{RDS}} F}{2.303RT}(E^{\circ\prime}_E - E^{\circ\prime}_D) \qquad (8)$$

We assumed that $\Gamma_{E,eff}$ was constant at all pH values because the conditions for enzyme modification were uniform. Equation (8) can be rewritten to as shown in Equation (9).

$$\log\left(\frac{j_{\mathrm{cat}}}{\mathrm{mA\ cm^{-2}}}\right) = \frac{\gamma n_{\mathrm{RDS}} F}{2.303RT}(E^{\circ\prime}_E - E^{\circ\prime}_D) + \log\left(\frac{n_S F k_{\mathrm{DET},0}\Gamma_{E,\mathrm{eff}}}{\mathrm{mA\ cm^{-2}}}\right) \qquad (9)$$

Equation (9) shows that log (j_{cat} / mA cm^{-2}) depends linearly on $E^{\circ\prime}_E - E^{\circ\prime}_D$, and the slope ($\gamma n_{RDS}F/2.303RT$) has an ideal value of 8.45 V^{-1}. Similar relationships were previously discussed for MET-type reactions, focusing on the formal potential of mediators ($E^{\circ\prime}_M$), and an LFER between $E^{\circ\prime}_M - E^{\circ\prime}_D$ and the bi-molecular reaction rate constant was demonstrated.[82–85] Equation (9) was fitted to the linear increasing region in the plot of log (j_{cat} / mA cm^{-2}) vs. $E^{\circ\prime}_E - E^{\circ\prime}_D$ using the least-squares analysis in Gnuplot®. Figure 7 shows the fitting results for both enzymes.

In the case of rALDH, the slope and γ were calculated to be 6.0 ± 0.4 V^{-1} and 0.35 ± 0.02, respectively, from the linear range (0.4–0.5 V), indicating that an ideal LFER was not observed. There is a possibility that the catalytic constant of rALDH is controlled by multiple RDSs due to the complicated ET pathway via the hemes *c* in the C subunit. Apparently, in the case of ΔC_ALDH, a linear increasing region between 0.3 and 0.5 V was observed. The slope and γ were calculated to be 8.3 ± 0.4 V^{-1} and 0.49 ± 0.03 (which is almost equal to 0.5 for an ideal LFER), respectively. This indicates that there are no specific interactions in the intramolecular ET, which is attributed to the simplification of the ET pathway due to the deletion of the C subunit. In the LFER region, k_{DET} was controlled by the potential difference in the ET pathway, and there was only one electron involved in the RDS. Apparently, log (j_{cat} / mA cm^{-2}) exhibited a constant value between 0.5 and 0.7 V, suggesting that $E^{\circ\prime}_E - E^{\circ\prime}_D$ was sufficiently large and the RDS was controlled by non-thermodynamic factors. Based on the structural information of ΔC_ALDH, the RDS in the intramolecular ET pathway can be summarized as follows:

1. In the LFER region, the RDS is estimated to be a 1-electron intramolecular ET process (Moco → [2Fe-2S]$_2$ or [2Fe-2S]$_2$ → [2Fe-2S]$_1$).

2. In the non-LFER region, k_{DET} is limited by other factors, such as catalytic turnover in Moco, entry of the substrate into the catalytic site, and potential-independent intramolecular ET.

We attempted to investigate the LFER of ΔC_ALDH based on the serial resistance model.[85] Assuming that k_{DET} is controlled by the potential difference between the LFER and non-LFER regions, k_{DET} can be expressed using Equation (10).

$$\frac{1}{k_{\mathrm{DET}}} = \frac{1}{k_{\mathrm{DET,LFER}}} + \frac{1}{k_{\mathrm{DET,non-LFER}}} \qquad (10)$$

where $k_{DET,LFER}$ and $k_{DET,non-LFER}$ are the catalytic constants in the DET-type bioelectrocatalysis controlled by the potential difference and other factors, respectiv

ely. The latter is the substantial limit of k_{DET}. Using Equations (3), (8), and (10), j_{cat} can be expressed using Equation (11).

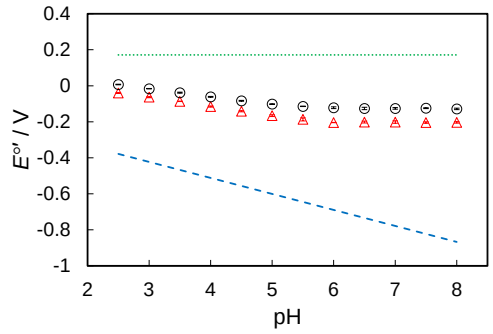

Figure 6. pH dependence of $E^{\circ\prime}_E$ of rALDH (circles) and ΔC_ALDH (triangles) and the formal potentials of the electron donor ($E^{\circ\prime}_D$ (broken blue line)) and an artificial electron acceptor ($E^{\circ\prime}_A$ (dotted green line)). Errors were determined using the Student's *t* distribution at 90% confidence level (n = 6).

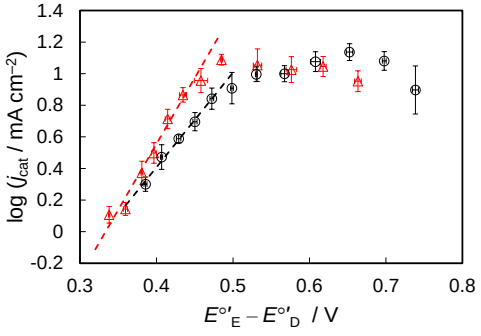

Figure 7. Plots of log (j_{cat} / mA cm^{-2}) vs. $E^{\circ\prime}_E - E^{\circ\prime}_D$ for rALDH (black) and ΔC_ALDH (red). The circles and triangles indicate the experimental values of rALDH and ΔC_ALDH, respectively. The broken lines indicate the fitted lines (Equation (9)). Errors were determined using the Student's *t* distribution at 90% confidence level (n = 6).

$$j_{\mathrm{cat}} = \left[\frac{1}{n_{\mathrm{S}} F k_{\mathrm{DET},0} \Gamma_{\mathrm{E,eff}} \exp\left\{ \frac{\gamma n_{\mathrm{RDS}} F}{RT} \left(E^{\circ\prime}{}_{\mathrm{E}} - E^{\circ\prime}{}_{\mathrm{D}} \right) \right\}} + \frac{1}{n_{\mathrm{S}} F k_{\mathrm{DET,non-LFER}} \Gamma_{\mathrm{E,eff}}} \right]^{-1} \tag{11}$$

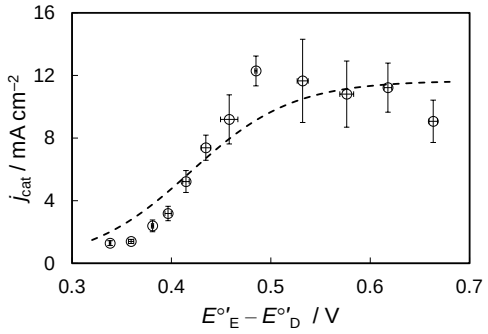

Figure 8. Fitting curve for the plot of j_{cat} vs. $E^{\circ\prime}{}_{\mathrm{E}} - E^{\circ\prime}{}_{\mathrm{D}}$ for ΔC_ALDH (broken line; Equation (11)). The open circles indicate the experimental values. Errors were determined using the Student's t distribution at 90% confidence level (n = 6).

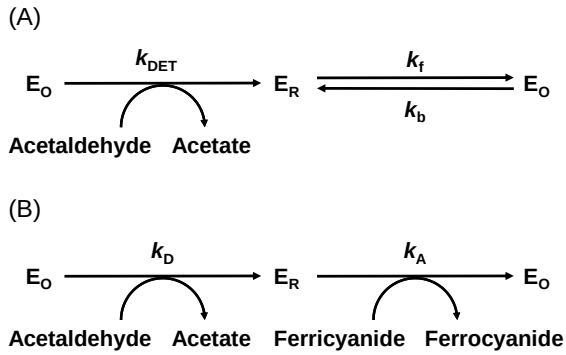

Scheme 1. (A) Catalytic cycles of ALDH in the DET-type reaction and (B) the coupled reaction of acetaldehyde oxidation and ferricyanide reduction based on the ping-pong Bi Bi mechanism. E_O and E_R indicate the oxidized and reduced states of the enzyme, respectively. k_f and k_b are the surface ET rate constants expressed using the Butler–Volmer equation shown below:

$$k_{\mathrm{f}} = k^{\circ} \exp\left\{ \frac{(1-\alpha) n'_{\mathrm{E}} F}{RT} \left(E - E^{\circ\prime}{}_{\mathrm{E}} \right) \right\},$$

$$k_{\mathrm{b}} = k^{\circ} \exp\left\{ -\frac{\alpha n'_{\mathrm{E}} F}{RT} \left(E - E^{\circ\prime}{}_{\mathrm{E}} \right) \right\}$$

Using $k_{\mathrm{DET},0}\,\Gamma_{\mathrm{E,eff}}$ and $k_{\mathrm{DET,non\text{-}LFER}}\,\Gamma_{\mathrm{E,eff}}$ as adjustable parameters, Equation (11) was fitted to the plot of j_{cat} vs. $E^{\circ\prime}{}_{\mathrm{E}} - E^{\circ\prime}{}_{\mathrm{D}}$ by non-linear least-squares analysis in Gnuplot®, fixing the value of γ as 0.5. The fitting results are shown in Figure 8. The values of $k_{\mathrm{DET},0}\,\Gamma_{\mathrm{E,eff}}$ and $k_{\mathrm{DET,non\text{-}LFER}}\,\Gamma_{\mathrm{E,eff}}$ were calculated to be 17 ± 2 and 60000 ± 2000 pmol cm^{-2} s^{-1}, respectively. To separately evaluate the obtained parameters ($k_{\mathrm{DET},0}$, $k_{\mathrm{DET,non\text{-}LFER}}$, and $\Gamma_{\mathrm{E,eff}}$), we investigated the enzymatic properties using another electron acceptor in the next section.

3.3. Enzyme characterization considering ferricyanide reductase activity in solution. The solution activities of rALDH and ΔC_ALDH were investigated using ferricyanide as an alternative electron acceptor instead of an electrode. Figure 9 shows the ferricyanide reductase activities of both enzymes in solution (k_{sol}). Compared with the DET activity, the k_{sol} of rALDH exhibited a completely different pH dependence, with a maximum value at pH 4.0. This suggests that the k_{sol} of rALDH does not follow thermodynamics and is controlled by specific interactions between the enzyme and ferricyanide, such as electrostatic and hydrophobic interactions. In contrast, the k_{sol} of ΔC_ALDH has a similar pH dependence to the DET-type reaction.

Assuming that the specific interaction between ΔC_ALDH and ferricyanide is negligible, we attempted to kinetically analyze the relationship between the potential difference and k_{sol} of ΔC_ALDH based on the LFER. Based on the ping-pong Bi Bi mechanism, the catalytic cycles of ALDH in the DET-type reaction and the coupled reaction of acetaldehyde oxidation and ferricyanide reduction are shown in Scheme 1, in which, k_{D} and k_{A} are the catalytic constants for donor (acetaldehyde) oxidation and acceptor (ferricyanide) reduction, respectively. Based on the similarity of the electron donors and acceptors shown in Schemes 1A and 1B, k_{DET} can be regarded as an upstream of k_{sol} and equal to k_{D}. k_{sol} can be expressed using Equation (12).

$$\frac{1}{k_{\mathrm{sol}}} = \frac{1}{k_{\mathrm{DET}}} + \frac{1}{k_{\mathrm{A}}} \tag{12}$$

We assumed that k_{A} comprised potential-dependent and independent terms and that the potential-dependent term of k_{A} followed the LFER and was controlled by $E^{\circ\prime}{}_{\mathrm{A}} - E^{\circ\prime}{}_{\mathrm{E}}$. As shown in Equations (8) and (10), k_{DET} and k_{A} are expressed using Equations (13) and (14), respectively.

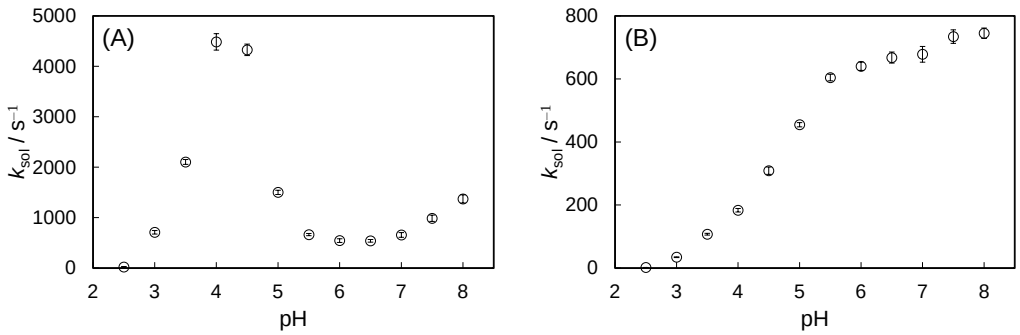

Figure 9. Ferricyanide reductase activities of (A) rALDH and (B) ΔC_ALDH in solution. Errors were determined using the Student's t distribution at 90% confidence level (n = 6).

$$\frac{1}{k_{\mathrm{DET}}} = \frac{1}{k_{\mathrm{DET,0}} \exp\left\{\frac{\gamma n_{\mathrm{RDS}} F}{RT}\left(E^{\circ\prime}_{\mathrm{E}} - E^{\circ\prime}_{\mathrm{D}}\right)\right\}} + \frac{1}{k_{\mathrm{DET,non-LFER}}} \tag{13}$$

$$\frac{1}{k_{\mathrm{A}}} = \frac{1}{k_{\mathrm{A,0}} \exp\left\{\frac{\gamma' n'_{\mathrm{RDS}} F}{RT}\left(E^{\circ\prime}_{\mathrm{A}} - E^{\circ\prime}_{\mathrm{E}}\right)\right\}} + \frac{1}{k_{\mathrm{A,non-LFER}}} \tag{14}$$

where γ and n_{RDS} are 0.5 and 1, respectively, using the results in Section 3.2. Similarly, γ' and n'_{RDS} were assumed to be 0.5 and 1, respectively. $E^{\circ\prime}_{\mathrm{E}} - E^{\circ\prime}_{\mathrm{D}}$ and $E^{\circ\prime}_{\mathrm{A}} - E^{\circ\prime}_{\mathrm{E}}$ changed with pH, as shown in Figure 6. Using Equations (12), (13), and (14), k_{sol} can be obtained as shown in Equation (15).

$$k_{\mathrm{sol}} = \left[\frac{1}{k_{\mathrm{DET,0}} \exp\left\{\frac{\gamma n_{\mathrm{RDS}} F}{RT}\left(E^{\circ\prime}_{\mathrm{E}} - E^{\circ\prime}_{\mathrm{D}}\right)\right\}} + \frac{1}{k_{\mathrm{A,0}} \exp\left\{\frac{\gamma' n'_{\mathrm{RDS}} F}{RT}\left(E^{\circ\prime}_{\mathrm{A}} - E^{\circ\prime}_{\mathrm{E}}\right)\right\}} + \frac{1}{k_{\mathrm{sol,non-LFER}}}\right]^{-1} \tag{15}$$

$k_{\mathrm{sol,non\text{-}LFER}}$ can be defined as shown in Equation (16).

$$\frac{1}{k_{\mathrm{sol,non-LFER}}} = \frac{1}{k_{\mathrm{DET,non-LFER}}} + \frac{1}{k_{\mathrm{A,non-LFER}}} \tag{16}$$

Using $k_{\mathrm{DET,0}}$, $k_{\mathrm{A,0}}$, and $k_{\mathrm{sol,non\text{-}LFER}}$ as adjustable parameters, Equation (15) was fitted to a 3D surface representing the relationship among $E^{\circ\prime}_{\mathrm{E}} - E^{\circ\prime}_{\mathrm{D}}$, $E^{\circ\prime}_{\mathrm{A}} - E^{\circ\prime}_{\mathrm{E}}$, and k_{sol}. The fitting results are shown in Figure 10. The $k_{\mathrm{DET,0}}$, $k_{\mathrm{A,0}}$, and $k_{\mathrm{sol,non\text{-}LFER}}$ values were calculated to be 1.4 ± 0.7, 0.93 ± 0.08, and 1500 ± 100 s^{-1}, respectively. $\Gamma_{\mathrm{E,eff}}$ was calculated to be 13 ± 7 pmol cm^{-2} from the value of $k_{\mathrm{DET,0}}\,\Gamma_{\mathrm{E,eff}}$ provided in Section 3.2. The peak current density of the 1-electron reversible non-catalytic signal (j_{p}) is theoretically expressed as $|j_{\mathrm{p}}| = F^2 v \Gamma_{\mathrm{E,eff}}/4RT$;[9] therefore, the $\Gamma_{\mathrm{E,eff}}$ value corresponds to $|j_{\mathrm{p}}|$ = 120 ± 60 nA cm^{-2} at v = 10 mV s^{-1}, which is consistent with the result that the non-catalytic signal of ΔC_ALDH could not be observed. $k_{\mathrm{DET,non\text{-}LFER}}$ and $k_{\mathrm{A,non\text{-}LFER}}$ were calculated to be 5000 ± 2000 and 2200 ± 600 s^{-1}, respectively. Because $k_{\mathrm{DET,non\text{-}LFER}}$ was larger than $k_{\mathrm{A,non\text{-}LFER}}$, the catalytic activity in solution was partly affected by the non-LFER factors involved in the electron acceptor. $k_{\mathrm{DET,non\text{-}LFER}}$ is the maximum catalytic constant that is independent of the thermodynamic parameters, and its value is consistent with previous reports, in which, catalytic constants of 10^3 s^{-1} were obtained for other metalloenzymes.[86,87] The pH dependence of k_{DET} and k°_{max} was calculated separately, as shown in Figure 11.

From the comparison of the catalytic processes between the DET-type and ferricyanide reductase reactions, $\Gamma_{\mathrm{E,eff}}$ and k_{DET} were separately obtained without non-catalytic signals. Reactions involving an alternative electron acceptor (or donor) are partly controlled by the kinetics between the enzymes and acceptor (or donor), as expressed in Equation (14). We conclude that DET-type reactions are effective for solely evaluating the kinetics of substrate oxidation (or reduction).

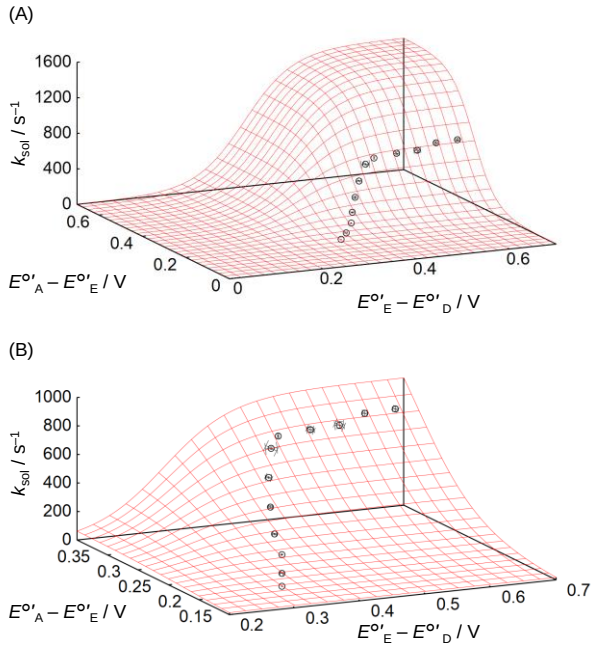

Figure 10. Fitting surface for the 3D plot representing the relationship among $E^{\circ\prime}_{\mathrm{E}} - E^{\circ\prime}_{\mathrm{D}}$, $E^{\circ\prime}_{\mathrm{A}} - E^{\circ\prime}_{\mathrm{E}}$, and k_{sol} of ΔC_ALDH (red lines; Equation (15)). The open circles indicate the experimental values. (A): Overall and (B): enlarged views. Errors were determined using the Student's t distribution at 90% confidence level (n = 6).

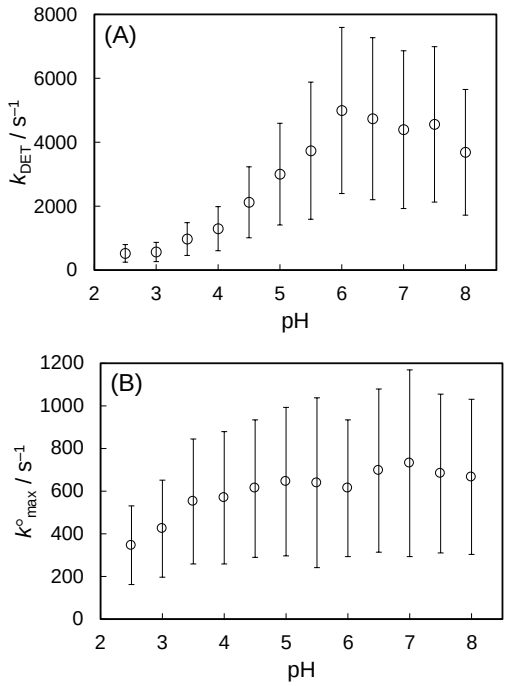

Figure 11. pH dependence of (A) k_{DET} and (B) k°_{max}. Errors were determined using the Student's t distribution at 90% confidence level (n = 6).

4. CONCLUSIONS

DET activity of ΔC_ALDH was evidently observed at the MWCNT electrodes. Compared with rALDH, ΔC_ALDH exhibited advantages of decreasing the overpotential and simplifying the ET pathway. Based on the aforementioned bioelectrochemical discussions, the catalytic constant of ΔC_ALDH comprised potential-dependent and independent processes in both the DET-type and ferricyanide reductase reactions. The two reactions with the different electron acceptors were kinetically analyzed, and $\Gamma_{E,eff}$ and k_{DET} were separately evaluated without non-catalytic signals. Moreover, the DET-type reaction was useful for evaluating the catalytic cycle without considering the interactions with other electron acceptors or donors. We also demonstrated that the potential difference between the substrate and enzyme is an essential factor in determining catalytic activity. This study could be useful for developing novel methods for enzyme characterization and enzymes with high catalytic activity.

ASSOCIATED CONTENT

Supporting Information

SDS-PAGE of the enzymes, bacterial strains, plasmids, primers, and additional structural and electrochemical data are described in Supporting Information.

AUTHOR INFORMATION

Corresponding Authors

Taiki Adachi – Division of Applied Life Sciences, Graduate School of Agriculture, Kyoto University, Sakyo, Kyoto 606-8502, Japan, orcid.org/0000-0002-3863-993X; E-mail: adachi.taiki.5z@kyoto-u.ac.jp

Keisei Sowa – Division of Applied Life Sciences, Graduate School of Agriculture, Kyoto University, Sakyo, Kyoto 606-8502, Japan, orcid.org/0000-0001-9767-4922; E-mail: sowa.keisei.2u@kyoto-u.ac.jp

Authors

Konatsu Ichikawa – Division of Applied Life Sciences, Graduate School of Agriculture, Kyoto University, Sakyo, Kyoto 606-8502, Japan

Yuki Kitazumi – Division of Applied Life Sciences, Graduate School of Agriculture, Kyoto University, Sakyo, Kyoto 606-8502, Japan

Osamu Shirai – Division of Applied Life Sciences, Graduate School of Agriculture, Kyoto University, Sakyo, Kyoto 606-8502, Japan

Funding Sources

JSPS KAKENHI (Grant Numbers JP23K19281 and JP22K14831). FY 2022 Kusunoki 125 of Kyoto University 125th Anniversary Fund. GteX Program of Japan (Grant Number JPMJGX23B4).

Notes

The authors declare no competing financial interest.

ACKNOWLEDGMENTS

This research was supported by JSPS KAKENHI Grant Numbers JP23K19281 to T.A. and JP22K14831 to K.S., and FY 2022 Kusunoki 125 of Kyoto University 125th Anniversary Fund to K.S. This study was supported by the GteX Program of Japan Grant Number JPMJGX23B4 to K.S. We express our deep gratitude to Mr. Hirou Kaku, Mr. Koryu Ou, and Mr. Yasuyuki Hamano for providing financial support to K.S.. We would also like to thank Editage (www.editage.com) for the English language editing.

ABBREVIATIONS

ADH, alcohol dehydrogenase; ALDH, aldehyde dehydrogenase; BCA, bicinchoninic acid; ΔC_AlDH, variant of ALDH without the cytochrome *c* subunit; CV, cyclic voltammogram; DET, direct electron transfer; DNA, deoxyribonucleic acid; ET, electron transfer; FDH, fructose dehydrogenase; FeS, iron-sulfur cluster; GCE, glassy carbon electrode; GDH, glucose dehydrogenase; LFER, linear free energy relationship; MET, mediated electron transfer; Moco, molybdenum cofactor; MWCNT, multi-walled carbon nanotube; NMP, *N*-methyl-2-pyrrolidone; PCR, polymerase chain reaction; rALDH, wild-type recombinant ALDH; RDS, rate-determining step; SDS-PAGE, sodium dodecyl sulfate polyacrylamide gel electrophoresis.

REFERENCES

(1) Scheller, F.; Kirstein, D.; Kirstein, L.; Schubert, F.; Wollenberger, U.; Olsson, B.; Gorton, L.; Johansson, G. Enzyme Electrodes and Their Application. *Phil. Trans. R. Soc. Lond. B.* **1987**, *316* (1176), 85–94. https://doi.org/10.1098/rstb.1987.0019.

(2) Willner, I.; Katz, E.; Willner, B. Electrical Contact of Redox Enzyme Layers Associated with Electrodes: Routes to Amperometric Biosensors. *Electroanalysis* **1997**, *9* (13), 965–977. https://doi.org/10.1002/elan.1140091302.

(3) Bartlett, P. N. Bioelectrochemistry: Fundamentals, Experimental Techniques and Applications. John Wiley & Sons, Chichester **2008**. https://doi.org/10.1002/9780470753842.

(4) Armstrong, F. A.; Hirst, J. Reversibility and Efficiency in Electrocatalytic Energy Conversion and Lessons from Enzymes. *Proc. Natl. Acad. Sci. U. S. A.* **2011**, *108* (34), 14049–14054. https://doi.org/10.1073/pnas.1103697108.

(5) Fourmond, V.; Léger, C. Modelling the Voltammetry of Adsorbed Enzymes and Molecular Catalysts. *Curr. Opin. Electrochem.* **2017**, *1* (1), 110–120. https://doi.org/10.1016/j.coelec.2016.11.002.

(6) Yates, N. D. J.; Fascione, M. A.; Parkin, A. Methodologies for "Wiring" Redox Proteins/Enzymes to Electrode Surfaces. *Chem. Eur. J.* **2018**, *24* (47), 12164–12182. https://doi.org/10.1002/chem.201800750.

(7) Adachi, T.; Kitazumi, Y.; Shirai, O.; Kano, K. Recent Progress in Applications of Enzymatic Bioelectrocatalysis. *Catalysts* **2020**, *10* (12), 1413. https://doi.org/10.3390/catal10121413.

(8) Lojou, E.; Xiao, X. Enzymatic Bioelectrocatalysis. *Catalysts* **2021**, *11* (11), 1373. https://doi.org/10.3390/catal11111373.

(9) Léger, C.; Bertrand, P. Direct Electrochemistry of Redox Enzymes as a Tool for Mechanistic Studies. *Chem. Rev.* **2008**, *108* (7), 2379–2438. https://doi.org/10.1021/cr0680742.

(10) Sensi, M.; del Barrio, M.; Baffert, C.; Fourmond, V.; Léger, C. New Perspectives in Hydrogenase Direct Electrochemistry. *Curr. Opin. Electrochem.* **2017**, *5* (1), 135–145. https://doi.org/10.1016/j.coelec.2017.08.005.

(11) Milton, R. D.; Minteer, S. D. Direct Enzymatic Bioelectrocatalysis: Differentiating between Myth and Reality. *J. R. Soc. Interface* **2017**, *14* (131), 20170253. https://doi.org/10.1098/rsif.2017.0253.

(12) Bollella, P.; Gorton, L.; Antiochia, R. Direct Electron Transfer of Dehydrogenases for Development of 3rd Generation Biosensors and Enzymatic Fuel Cells. *Sensors* **2018**, *18* (5), 1319. https://doi.org/10.3390/s18051319.

(13) Adachi, T.; Kitazumi, Y.; Shirai, O.; Kano, K. Direct Electron Transfer-Type Bioelectrocatalysis of Redox Enzymes at Nanostructured Electrodes. *Catalysts* **2020**, *10* (2), 236. https://doi.org/10.3390/catal10020236.

(14) Armstrong, F. A. Some Fundamental Insights into Biological Redox Catalysis from the Electrochemical Characteristics of Enzymes Attached Directly to Electrodes. *Electrochim. Acta* **2021**, *390* (10), 138836. https://doi.org/10.1016/j.electacta.2021.138836.
(15) Gorton, L.; Jönsson-Pettersson, G.; Csöregi, E.; Johansson, K.; Domínguez, E.; Marko-Varga, G. Amperometric Biosensors Based on an Apparent Direct Electron Transfer between Electrodes and Immobilized Peroxidases. Plenary Lecture. *Analyst* **1992**, *117* (8), 1235–1241. https://doi.org/10.1039/AN9921701235.
(16) Lobo, M. J.; Miranda, A. J.; Tuñón, P. Amperometric Biosensors Based on NAD(P)-Dependent Dehydrogenase Enzymes. *Electroanalysis* **1997**, *9* (3), 191–202. https://doi.org/10.1002/elan.1140090302.
(17) Xu, C. X.; Marzouk, S. A. M.; Cosofret, V. V.; Buck, R. P.; Neuman, M. R.; Sprinkle, R. H. Development of a Diamine Biosensor. *Talanta* **1997**, *44* (9), 1625–1632. https://doi.org/10.1016/S0039-9140(97)00067-2.
(18) Thévenot, D. R.; Toth, K.; Durst, R. A.; Wilson, G. S. Electrochemical Biosensors: Recommended Definitions and Classification. *Biosens. Bioelectron.* **2001**, *16* (1–2), 121–131. https://doi.org/10.1016/s0956-5663(01)00115-4.
(19) Scheller, F.; Schubert, F.; Pfeiffer, D.; Hintsche, R.; Dransfeld, I.; Renneberg, R.; Wollenberger, U.; Riedel, K.; Pavlova, M.; Kühn, M.; Müller, H.-G.; Tan, P. M.; Hoffmann, W.; Moritz, W. Research and Development of Biosensors. A Review. *Analyst* **1989**, *114* (6), 653–662. https://doi.org/10.1039/AN9891400653.
(20) Avramescu, A.; Noguer, T.; Magearu, V.; Marty, J.-L. Chronoamperometric Determination of d-Lactate Using Screen-Printed Enzyme Electrodes. *Anal. Chim. Acta* **2001**, *433* (1), 81–88. https://doi.org/10.1016/S0003-2670(00)01386-6.
(21) Martinkova, P.; Kostelnik, A.; Valek, T.; Pohanka, M. Main Streams in the Construction of Biosensors and Their Applications. *Int. J. Electrochem. Sci.* **2017**, *12* (8), 7386–7403. http://doi.org/10.20964/2017.08.02.
(22) Bollella, P.; Gorton, L. Enzyme Based Amperometric Biosensors. *Curr. Opin. Electrochem.* **2018**, *10*, 157–173. https://doi.org/10.1016/j.coelec.2018.06.003.
(23) Bollella, P.; Hibino Y.; Kano, K.; Gorton L.; Antiochia R. Highly Sensitive Membraneless Fructose Biosensor Based on Fructose Dehydrogenase Immobilized onto Aryl Thiol Modified Highly Porous Gold Electrode: Characterization and Application in Food Samples. *Anal. Chem.* **2018**, *90* (20), 12131–12136. https://doi.org/10.1021/acs.analchem.8b03093.
(24) Kucherenko, I. S.; Soldatkin, O. O.; Kucherenko, D. Y.; Soldatkina, O. V.; Dzyadevych, S. V. Advances in Nanomaterial Application in Enzyme-Based Electrochemical Biosensors: A Review. *Nanoscale Adv.* **2019**, *1*, 4560–4577. https://doi.org/10.1039/C9NA00491B.
(25) Nguyen, H. H.; Lee, S. H.; Lee, U. J.; Fermin, C. D.; Kim, M. Immobilized Enzymes in Biosensor Applications. *Materials* **2019**, *12* (1), 121. https://doi.org/10.3390/ma12010121.
(26) Bollella, P.; Katz, E. Enzyme-Based Biosensors: Tackling Electron Transfer Issues. *Sensors* **2020**, *20* (12), 3517. https://doi.org/10.3390/s20123517.
(27) Pinyou, P.; Blay, V.; Muresan, L. M.; Noguer, T. Enzyme-Modified Electrodes for Biosensors and Biofuel Cells. *Mater. Horiz.* **2019**, *6* (7), 1336–1358. https://doi.org/10.1039/C9MH00013E.
(28) Barton, S. C.; Gallaway, J.; Atanassov, P. Enzymatic Biofuel Cells for Implantable and Microscale Devices. *Chem. Rev.* **2004**, *104* (10), 4867–4886. https://doi.org/10.1021/cr020719k.
(29) Cracknell, J. A.; Vincent, K. A.; Armstrong, F. A. Enzymes as Working or Inspirational Electrocatalysts for Fuel Cells and Electrolysis. *Chem. Rev.* **2008**, *108* (7), 2439–2461. https://doi.org/10.1021/cr0680639.
(30) Meredith, M. T.; Minteer, S. D. Biofuel Cells: Enhanced Enzymatic Bioelectrocatalysis. *Annu. Rev. Anal. Chem.* **2012**, *5*, 157–179. https://doi.org/10.1146/annurev-anchem-062011-143049.
(31) de Poulpiquet, A.; Ranava, D.; Monsalve, K.; Giudici-Orticoni, M.-T.; Lojou, E. Biohydrogen for a New Generation of H_2/O_2 Biofuel Cells: A Sustainable Energy Perspective. *ChemElectroChem* **2014**, *1* (11), 1724–1750. https://doi.org/10.1002/celc.201402249.
(32) Mazurenko, I.; de Poulpiquet, A.; Lojou, E. Recent Developments in High Surface Area Bioelectrodes for Enzymatic Fuel Cells. *Curr. Opin. Electrochem.* **2017**, *5* (1), 74–84. https://doi.org/10.1016/j.coelec.2017.07.001.
(33) Mano, N.; de Poulpiquet, A. O_2 Reduction in Enzymatic Biofuel Cells. *Chem. Rev.* **2018**, *118* (5), 2392–2468. https://doi.org/10.1021/acs.chemrev.7b00220.
(34) Xiao, X.; Xia, H.-Q.; Wu, R.; Bai, L.; Yan, L.; Magner, E.; Cosnier, S.; Lojou, E.; Zhu, Z.; Liu, A. Tackling the Challenges of Enzymatic (Bio)Fuel Cells. *Chem. Rev.* **2019**, *119* (16), 9509–9558. https://doi.org/10.1021/acs.chemrev.9b00115.
(35) Carsol, M.-A.; Mascini, M. Diamine Oxidase and Putrescine Oxidase Immobilized Reactors in Flow Injection Analysis: A Comparison in Substrate Specificity. *Talanta* **1999**, *50* (1), 141–148. https://doi.org/10.1016/s0039-9140(99)00111-3.
(36) Krieg, T.; Sydow, A.; Schröder, U.; Schrader, J.; Holtmann, D. Reactor Concepts for Bioelectrochemical Syntheses and Energy Conversion. *Trends Biotechnol.* **2014**, *32* (12), 645–655. https://doi.org/10.1016/j.tibtech.2014.10.004.
(37) Milton, R. D.; Minteer, S. D. Enzymatic Bioelectrosynthetic Ammonia Production: Recent Electrochemistry of Nitrogenase, Nitrate Reductase, and Nitrite Reductase. *ChemPlusChem* **2017**, *82* (4), 513–521. https://doi.org/10.1002/cplu.201600442.
(38) Meneghello, M.; Léger, C.; Fourmond, V. Electrochemical Studies of CO_2-Reducing Metalloenzymes. *Chem. Eur. J.* **2021**, *27* (70), 17542–17553. https://doi.org/10.1002/chem.202102702.
(39) Can, M.; Armstrong, F. A.; Ragsdale, S. W. Structure, Function, and Mechanism of the Nickel Metalloenzymes, CO Dehydrogenase, and Acetyl-CoA Synthase. *Chem. Rev.* **2014**, *114* (8), 4149–4174. https://doi.org/10.1021/cr400461p.
(40) Adachi, T.; Kaida, Y.; Kitazumi, Y.; Shirai, O.; Kano, K. Bioelectrocatalytic performance of D-Fructose Dehydrogenase. *Bioelectrochemistry* **2019**, *129*, 1–9. https://doi.org/10.1016/j.bioelechem.2019.04.024.
(41) Kummer, M. J.; Minteer, S. D. Enzymatic Bioelectrocatalysis for Enzymology Applications. *ChemElectroChem* **2020**, *7* (10), 2222–2226. https://doi.org/10.1002/celc.202000239.
(42) Fukawa, E.; Suzuki, Y.; Adachi, T.; Miyata, T.; Makino, F.; Tanaka, H.; Namba, K.; Sowa, K.; Kitazumi, Y.; Shirai, O. Structural and Electrochemical Elucidation of Biocatalytic Mechanisms in Direct Electron Transfer-Type D-Fructose Dehydrogenase. *Electrochim. Acta* **2024**, *490*, 144271. https://doi.org/10.1016/j.electacta.2024.144271.
(43) Tsujimura, S.; Nakagawa, T.; Kano, K.; Ikeda, T. Kinetic Study of Direct Bioelectrocatalysis of Dioxygen Reduction with Bilirubin Oxidase at Carbon Electrodes. *Electrochemistry* **2004**, *72* (6), 437–439. https://doi.org/10.5796/electrochemistry.72.437.
(44) Bard, A. J.; Faulkner, L. R. Electrochemical Methods Fundamentals and Applications, 2nd ed; John Wiley & Sons: Hoboken, NJ, USA, 2001.
(45) Moser, C. C.; Keske, J. M.; Warncke, K.; Farid, R. S.; Dutton, P. L. Nature of Biological Electron Transfer. *Nature* **1992**, *355*, 796–802. https://doi.org/10.1038/355796a0.
(46) Siritanaratkul, B.; Megarity, C. F.; Roberts, T. G.; Samuels, T. O. M.; Winkler, M.; Warner, J. H.; Happe, T.; Armstrong, F. A. Transfer of Photosynthetic $NADP^+$/NADPH Recycling Activity to a Porous Metal Oxide for Highly Specific,

Electrochemically-Driven Organic Synthesis. *Chem. Sci.* **2017**, *8* (6), 4579–4586. https://doi.org/10.1039/C7SC00850C.
(47) So, K.; Kitazumi, Y.; Shirai, O.; Kano, K. Analysis of Factors Governing Direct Electron Transfer-Type Bioelectrocatalysis of Bilirubin Oxidase at Modified Electrodes. *J. Electroanal. Chem.* **2016**, *783* (15), 316–323. https://doi.org/10.1016/j.jelechem.2016.10.062.
(48) Léger, C.; Elliott, S. J.; Hoke, K. R.; Jeuken, L. J. C.; Jones, A. K.; Armstrong, F. A. Enzyme Electrokinetics: Using Protein Film Voltammetry to Investigate Redox Enzymes and Their Mechanisms. *Biochemistry* **2003**, *42* (29), 8653–8662. https://doi.org/10.1021/bi034789c.
(49) Sugimoto, Y.; Kitazumi, Y.; Shirai, O.; Kano, K. Effects of Mesoporous Structures on Direct Electron Transfer-Type Bioelectrocatalysis: Facts and Simulation on a Three-Dimensional Model of Random Orientation of Enzymes. *Electrochemistry* **2017**, *85* (2), 82–87. https://doi.org/10.5796/electrochemistry.85.82
(50) Adachi, O.; Tayama, K.; Shinagawa, E.; Matsushita, K.; Ameyama, M. Purification and Characterization of Membrane-Bound Aldehyde Dehydrogenase from *Gluconobacter suboxydans*. *Agric. Biol. Chem.* **1980**, *44* (3), 503–515. https://doi.org/10.1271/bbb1961.44.503.
(51) Prust, C.; Hoffmeister, M.; Liesegang, H.; Wiezer, A.; Fricke, W. F.; Ehrenreich, A.; Gottschalk, G.; Deppenmeier, U. Complete Genome Sequence of the Acetic Acid Bacterium *Gluconobacter oxydans*. *Nat. Biotechnol.* **2005**, *23* (2), 195–200. https://doi.org/10.1038/nbt1062.
(52) Tkac, J.; Svitel, J.; Vostiar, I.; Navratil, M.; Gemeiner, P. Membrane-Bound Dehydrogenases from *Gluconobacter* sp.: Interfacial Electrochemistry and Direct Bioelectrocatalysis. *Bioelectrochemistry* **2009**, *76* (1–2), 53–62. https://doi.org/10.1016/j.bioelechem.2009.02.013.
(53) Adachi, T.; Miyata, T.; Makino, F.; Tanaka, H.; Namba, K.; Kano, K.; Sowa, K.; Kitazumi, Y.; Osamu, S. Experimental and Theoretical Insights into Bienzymatic Cascade for Mediatorless Bioelectrochemical Ethanol Oxidation with Alcohol and Aldehyde Dehydrogenases. *ACS Catal*. **2023**, *13* (12), 7955–7965. https://doi.org/10.1021/acscatal.3c01962.
(54) Adachi, O.; Tayama, K.; Shinagawa, E.; Matsushita, K.; Ameyama, M. Purification and Characterization of Particulate Alcohol Dehydrogenase from *Gluconobacter suboxydans*. *Agric. Biol. Chem.* **1978**, *42* (11), 2045–2056. https://doi.org/10.1080/00021369.1978.10863306.
(55) Yakushi, T.; Matsushita, K. Alcohol Dehydrogenase of Acetic Acid Bacteria: Structure, Mode of Action, and Applications in Biotechnology. *Appl. Microbiol. Biotechnol.* **2010**, *86*, 1257–1265. https://doi.org/10.1007/s00253-010-2529-z.
(56) Kakehi, N.; Yamazaki, T.; Tsugawa, W.; Sode, K. A Novel Wireless Glucose Sensor Employing Direct Electron Transfer Principle Based Enzyme fuel Cell. *Biosens. Bioelectron*. **2007**, *22* (9–10), 2250–2255. https://doi.org/10.1016/j.bios.2006.11.004.
(57) Tsuya, T.; Ferri, S.; Fujikawa, M.; Yamaoka, H.; Sode, K. Cloning and Functional Expression of Glucose Dehydrogenase Complex of *Burkholderia Cepacia* in *Escherichia coli*. *J. Biotechnol.* **2006** *123* (2), 127–136. https://doi.org/10.1016/j.jbiotec.2005.10.017.
(58) Yamashita, Y.; Suzuki, N.; Hirose, N.; Kojima, K.; Tsugawa, W.; Sode, K. Mutagenesis Study of The Cytochrome *c* Subunit Responsible for The Direct Electron Transfer-Type Catalytic Activity of FAD-Dependent Glucose Dehydrogenase. *Int. J. Mol. Sci.* **2018**, *19* (4), 931. https://doi.org/10.3390/ijms19040931.
(59) Okuda-Shimazaki, J.; Yoshida, H.; Sode, K. FAD Dependent Glucose Dehydrogenases – Discovery and Engineering of Representative Glucose Sensing Enzymes. *Bioelectrochemistry* **2020**, *132*, 107414. https://doi.org/10.1016/j.bioelechem.2019.107414.
(60) Yoshida, H.; Kojima, K.; Shiota, M.; Yoshimatsu, K.; Yamazaki, T.; Ferri, S.; Tsugawa, W.; Kamitori, S.; Sode, K. X-Ray Structure of the Direct Electron Transfer-Type FAD Glucose Dehydrogenase Catalytic Subunit Complexed with a Hitchhiker Protein. *Acta Crystallogr. D: Struct. Biol.* **2019**, *75* (9), 841–851. https://doi.org/10.1107/s2059798319010878.
(61) Ikeda, T.; Matsushita, F.; Senda, M. Amperometric Fructose Sensor Based on Direct Bioelectrocatalysis. *Biosens. Bioelectron.* **1991**, *6* (4), 299–304. https://doi.org/10.1016/0956-5663(91)85015-O.
(62) Ameyama, M.; Shinagawa, E.; Matsushita, K.; Adachi, O. D-Fructose Dehydrogenase of *Gluconobacter Industrius*: Purification, Characterization, and Application to Enzymatic Microdetermination of D-Fructose. *J. Bacteriol.* **1981**, *145* (2), 814–823. https://doi.org/10.1128/jb.145.2.814-823.1981.
(63) Kawai, S.; Goda-Tsutsumi, M.; Yakushi, T.; Kano, K.; Matsushita, K. Heterologous Overexpression and Characterization of a Flavoprotein-Cytochrome c Complex Fructose Dehydrogenase of *Gluconobacter Japonicus* NBRC3260. *Appl. Environ. Microbiol.* **2013**, *79* (5), 1654–1660. https://doi.org/10.1128/AEM.03152-12.
(64) Suzuki, Y.; Makino, F.; Miyata, T.; Tanaka, H.; Namba, K.; Kano, K.; Sowa, K.; Kitazumi, Y.; Shirai, O. Essential Insight of Direct Electron Transfer-Type Bioelectrocatalysis by Membrane-Bound D-Fructose Dehydrogenase with Structural Bioelectrochemistry. *ACS Catal.* **2023**, *13* (20), 13828–13837. https://doi.org/10.1021/acscatal.3c03769.
(65) Matsushita, K.: Toshiharu, Y.; Toyama, H.; Shinagaw, E.; Adachi, O. Function of Multiple Heme *c* Moieties in Intramolecular Electron Transport and Ubiquinone Reduction in the Quinohemoprotein Alcohol Dehydrogenase-Cytochrome *c* Complex of *Gluconobacter suboxydans*. *J. Biol. Chem.* **1996**, *271* (9), 4850–4857. https://doi.org/10.1074/jbc.271.9.4850.
(66) Kawai, S.; Yakushi, T.; Matsushita, K.; Kitazumi, Y.; Shirai, O.; Kano, K. The Electron Transfer Pathway in Direct Electrochemical Communication of Fructose Dehydrogenase with Electrodes. *Electrochem. Commun.* **2014**, *38*, 28–31. https://doi.org/10.1016/j.elecom.2013.10.024.
(67) Kawai, S.; Kitazumi, Y.; Shirai, O.; Kano, K.; Bioelectrochemical Characterization of the Reconstruction of Heterotrimeric Fructose Dehydrogenase from Its Subunits. *Electrochim. Acta* **2016**, *210*, 689–694. https://doi.org/10.1016/j.electacta.2016.05.193.
(68) Suzuki, Y.; Sowa, K.; Kitazumi, Y.; Shirai, O. Enhancement of Direct Electron Transfer by Aromatic Thiol Modification with Truncated D-Fructose Dehydrogenase. *Electrochim. Acta* **2024**, *502*, 144804. https://doi.org/10.1016/j.electacta.2024.144804.
(69) Okuda-Shimazaki, J.; Loew, N.; Hirose, N.; Kojima, K.; Mori, K.; Tsugawa, W.; Sode, K. Construction and Characterization of Flavin Adenine Dinucleotide Glucose Dehydrogenase Complex Harboring a Truncated Electron Transfer Subunit. *Electrochim. Acta* **2018**, *277*, 276–286. https://doi.org/10.1016/j.electacta.2018.04.060.
(70) Lee, Y. S.; Baek, S.; Lee, H.; Reginald, S. S.; Kim, Y.; Kang, H.; Choi, I.-G.; Chang, I. S. Construction of Uniform Monolayer- and Orientation-Tunable Enzyme Electrode by a Synthetic Glucose Dehydrogenase without Electron-Transfer Subunit via Optimized Site-Specific Gold-Binding Peptide Capable of Direct Electron Transfer. *ACS Appl. Mater. Interfaces* **2018**, *10* (34), 28615–28626. https://doi.org/10.1021/acsami.8b08876.
(71) Lee, H.; Lee, Y. S.; Lee, S. K.; Baek, S.; Choi, I.-G.; Jang, J.-H.; Chang, I. S. Significant Enhancement of Direct Electric Communication across Enzyme-Electrode Interface via Nano-Patterning of Synthetic Glucose Dehydrogenase on Spatially Tunable Gold Nanoparticle (AuNP)-Modified Electrode. *Biosens. Bioelectron*. **2019**, *126*, 170–177. https://doi.org/10.1016/j.bios.2018.10.013.
(72) Lee, H.; Lee, E. M.; Reginald, S. S.; Chang, I. S. Peptide Sequence-Driven Direct Electron Transfer Properties and Binding Behaviors of Gold-Binding Peptide-Fused Glucose Dehydrogenase on Electrode. *iScience* **2021**, *24* (11), 103373. https://doi.org/10.1016/j.isci.2021.103373.

(73) Schäfer, A.; Tauch, A.; Jäger, W.; Kalinowski, J.; Thierbach, G. Pühler, A. Small Mobilizable Multi-Purpose Cloning Vectors Derived from the *Escherichia coli* Plasmids pK18 and pK19: Selection of Defined Deletions in the Chromosome of *Corynebacterium glutamicum*. *Gene*, **1994**, *145* (1), 69–73. https://doi.org/10.1016/0378-1119(94)90324-7.
(74) Figurski, D. H.; Helinski, D. R. Replication of an Origin-Containing Derivative of Plasmid RK2 Dependent on a Plasmid Function Provided in *trans*. *Proc. Natl. Acad. Sci. U. S A.* **1979**, *76* (4), 1648–1652. https://doi.org/10.1073/pnas.76.4.1648.
(75) Adachi, T.; Kitazumi, Y.; Shirai, O.; Kano, K. Direct Electron Transfer-Type Bioelectrocatalysis by Membrane-Bound Aldehyde Dehydrogenase from *Gluconobacter oxydans* and Cyanide Effects on Its Bioelectrocatalytic Properties. *Electrochem. Commun.* **2021**, *123*, 106911. https://doi.org/10.1016/j.elecom.2020.106911.
(76) Adachi, T.; Fujii, T.; Honda, M.; Kitazumi, Y.; Shirai, O.; Kano, K. Direct Electron Transfer-Type Bioelectrocatalysis of FAD-Dependent Glucose Dehydrogenase Using Porous Gold Electrodes and Enzymatically Implanted Platinum Nanoclusters. *Bioelectrochemistry* **2020**, *133*, 107457. https://doi.org/10.1016/j.bioelechem.2020.107457.
(77) Adachi, T.; Mazurenko, I.; Mano, N.; Kitazumi, Y.; Kataoka, K.; Kano, K.; Sowa, K.; Lojou, E. Kinetic and Thermodynamic Analysis of Cu^{2+}-Dependent Reductive Inactivation in Direct Electron Transfer-Type Bioelectrocatalysis by Copper Efflux Oxidase. *Electrochim. Acta* **2022**, *429*, 140987. https://doi.org/10.1016/j.electacta.2022.140987.
(78) Moser, C. C.; Anderson, J. L. R; Dutton, P. L. Guidelines for Tunneling in Enzymes. *Biochim. Biophys. Acta, Bioenerg.* **2010**, *1797* (9), 1573–1586. https://doi.org/10.1016/j.bbabio.2010.04.441.
(79) Kawai, S.; Yakushi, T.; Matsushita, K.; Kitazumi, Y.; Shirai, O.; Kano, K. Role of a Non-Ionic Surfactant in Direct Electron Transfer-Type Bioelectrocatalysis